Analysis techniques for adaptively controlled segmented mirror arrays

Gregory J. Michels*, Victor L. Genberg
Sigmadyne, 803 West Ave, Rochester, NY 14611
*michels@sigmadyne.com (585)235-6892

ABSTRACT

The employment of adaptively controlled segmented mirror architectures has become increasingly common in the development of current astronomical telescopes. Optomechanical analysis of such hardware presents unique issues as compared to that of monolithic mirror designs. Performance analysis issues include simulation of adaptive control, execution of polynomial fitting, calculation of best fit rigid body motions, and prediction of line-of-sight error. The generation of finite element models of individual segments involves challenges associated with correctly representing the geometry of the optical surface. Design issues include segment structural design optimization and optimum placement of actuators. Manufacturing issues include development of actuation inputs during stressed optic polishing. Approaches to all of the above issues are presented and demonstrated by example with SigFit, a commercially available tool integrating mechanical analysis with optical analysis.

Keywords: Integrated analysis, FEA, optomechanics, segmented optics, adaptive optics

1.0 INTRODUCTION

Many current telescope designs use adaptive, segmented optics in order to achieve large apertures otherwise infeasible with monolithic optics. Such systems present unique challenges and needs both in the development of the design and in the execution of performance analysis. This paper discusses some of these issues relating to creation of finite element models, analysis of adaptively controlled optics, surface deformation characterization, and design optimization. Implementation of the techniques discussed here is performed with SigFit[1], a software tool providing unique analysis capabilities for optical systems.

2.0 MODEL CREATION

The nature of segmented optics creates an opportunity for efficient model generation through a modeling technique known as slumping.[2] A technique is employed that simulates the process of the fabrication of the segment.

2.1 Geometry Characteristics of Off-Axis Segments

The mathematics of generating off-axis segments of an aspheric primary mirror are quite complicated. The complexity arises in that the calculation of surface sag expressed in the local segment coordinate system involves coordinate transformations and a root finding procedure as discussed below. Consider a segmented mirror with three rings of segments as shown in Figure 1. The segments within each ring have the same geometry, but vary from ring to ring as indicated by the alphabetic labels.

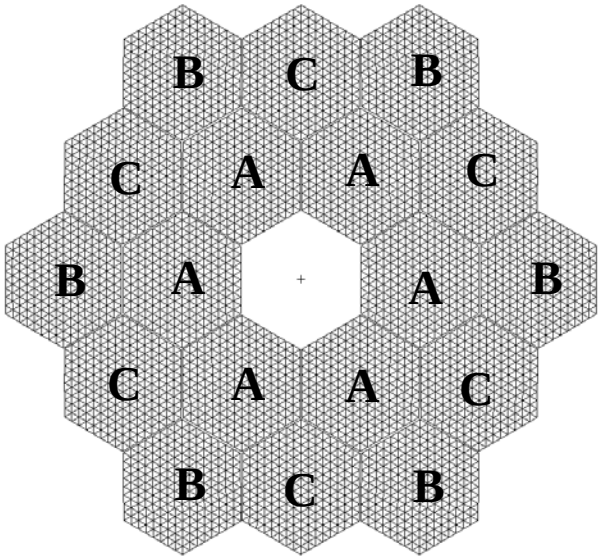

Figure 1: Segmented primary mirror with labels indicating identical segment geometries.

The three unique segments labeled A, B and C are shown in Figure 2 and Figure 3 with local coordinate systems whose Z axes are locally normal to the part centers.

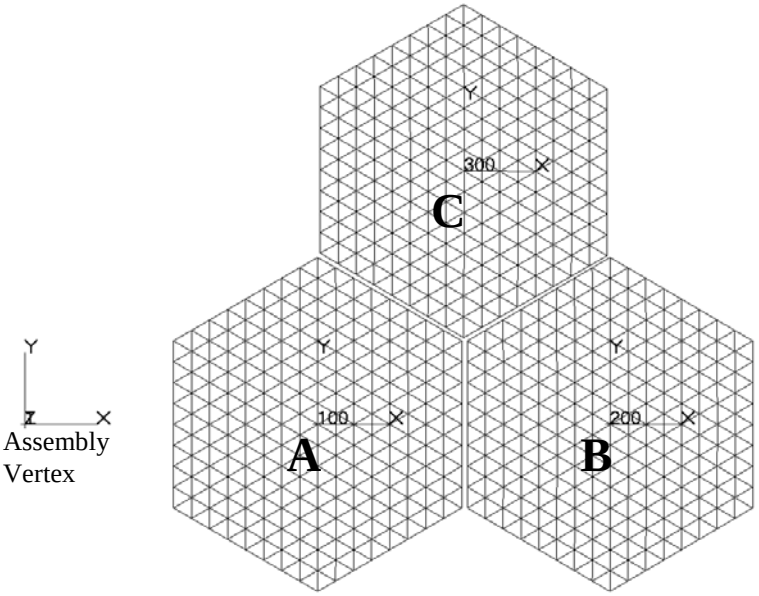

Figure 2: Top view of three unique segments A, B and C.

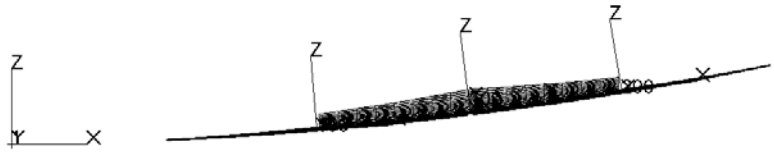

Figure 3: Side view of three unique segments A, B and C.

The aspheric sag measured parallel to the parent optical axis is shown in Figure 4 with a shaded contour plot over all three segments.

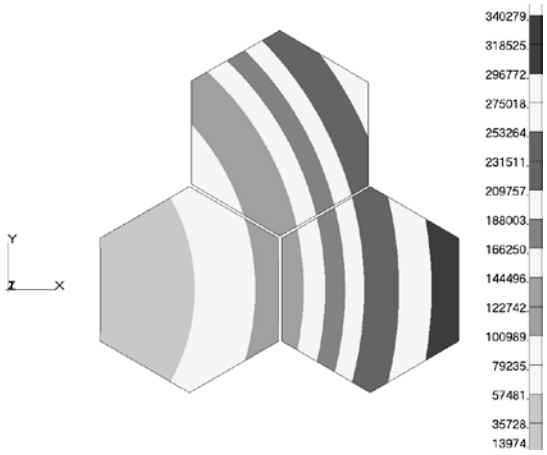

Figure 4: Global surface sag expressed in parent vertex coordinate system.

The local segment sag measured from a plane tangent to the parent asphere at each segment's center is shown in Figure 5. It is difficult to see the difference between segments in this plot since the power dominates the local prescriptions. However, after power has been removed, Figure 6 shows the differences in segment surface geometry.

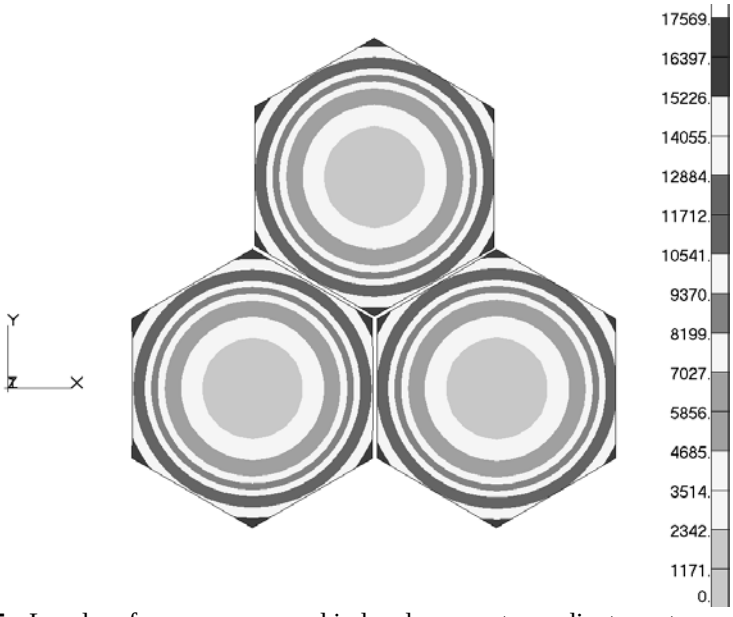

Figure 5: Local surface sag expressed in local segment coordinate systems.

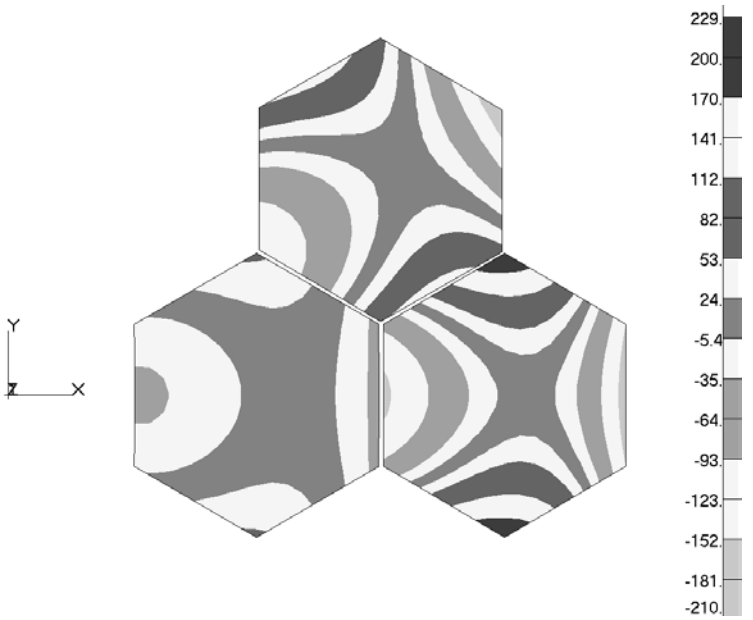

Figure 6: Local surface sag after power removed expressed in local segment coordinate systems.

2.2 Creation of Finite Element Models of Off-Axis Segments

The finite element models of these segments may be accurately constructed in a manner similar to a way in which the surfaces may be fabricated. In the fabrication process, the segment blanks may be initially figured with flat surfaces and then slumped to the geometry defined by the best-fit sphere. During the subsequent polishing cycles, the surface is then finished to the true aspheric geometry. This same process can be applied to the creation of the finite element model as shown in Figure 7. The process begins by creating a flat finite element model. Next all of the nodes of the flat model are slumped to the best-fit sphere in a direction along the axis of the segment centered coordinate system using the procedure presented in the previous section. Finally, the locations of only the optical surface nodes can then be adjusted to the exact aspheric geometry. This final adjustment in nodes requires finding the sag of the optical surface in the segment centered coordinate system, a process that requires some numerical root-finding techniques as discussed in the next subsection.

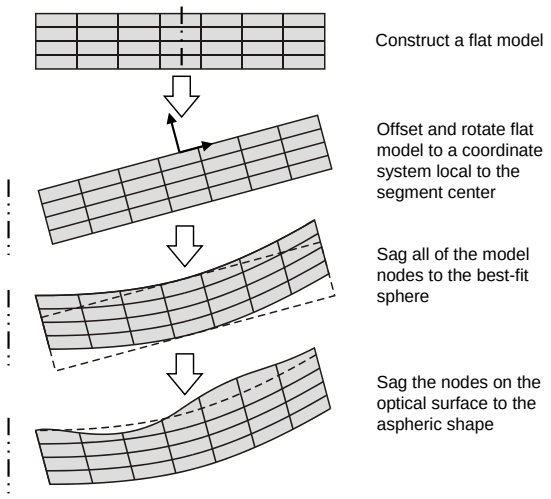

Figure 7: Process of slumping an off-axis segment model to an aspheric prescription.

The amount of adjustment of the surface nodes is usually very small, so there may be a negligible effect on deformation results due to mechanical loads. However, thermoelastic deformations are significantly affected by such small changes in shape representation.

2.3 Calculation of Local Segment Sag

It is often of interest to calculate the sag of a figured segment expressed in the Z axis of the local segment coordinate system such as those shown in Figure 2. The local segment sag is often used is the process of constructing finite element models through the use of the slumping technique described above. The local segment sag may also be used to obtain a polynomial fit of the segment surface geometry expressed in the local segment coordinate system. A polynomial fit of the surface geometry can be used in fabrication and testing of the segment. The reader may note that the Z axes of the local segment coordinate systems are not parallel to the Z axis of the parent vertex coordinate system centered on the segment array. This causes an iterative root finding process to be employed in order to compute the sag expressed in the local segment coordinate system. The steps required to calculate the sag as measured in the local segment coordinate system are as follows:

- Create a local segment coordinate system. For a given segment center with offset (x_0,y_0) find the corresponding segment center sag, z_0. Use (x_0,y_0,z_0) as the origin of the local segment coordinate system. Calculate the local normal to the vertex sag at this origin point to use as the direction of the Z axis of the local segment coordinate system.
- For any point on the segment tangent plane (x_s,y_s) measured in the local segment coordinate system the local segment sag, z_s, that locates the point (x_s,y_s,z_s) on the parent array surface is found. In this iterative root finding process x_s and y_s remain fixed while z_s is varied.
- The local segment locations may be used to define the segment model in the local segment coordinate system.

3.0 ADAPTIVE CONTROL ANALYSIS

3.1 Simulation of Adaptive Control

Adaptive control analysis will solve for the actuator strokes required to correct a deformed surface predicted by analysis.[3] The process of adaptive control analysis is illustrated in Figure 8 where an input disturbance is compensated by actuator influence functions each scaled by the actuator strokes, x_j. The analysis seeks to find xi such that the corrected surface RMS error is a minimum. If the actuator strokes are assumed to be unlimited then, the process of minimization of the corrected surface RMS error results in an unconstrained linear set of equations for the actuator strokes, x_i. The presence of stroke limits applies constraints to the solution requiring the use of linear programming techniques.

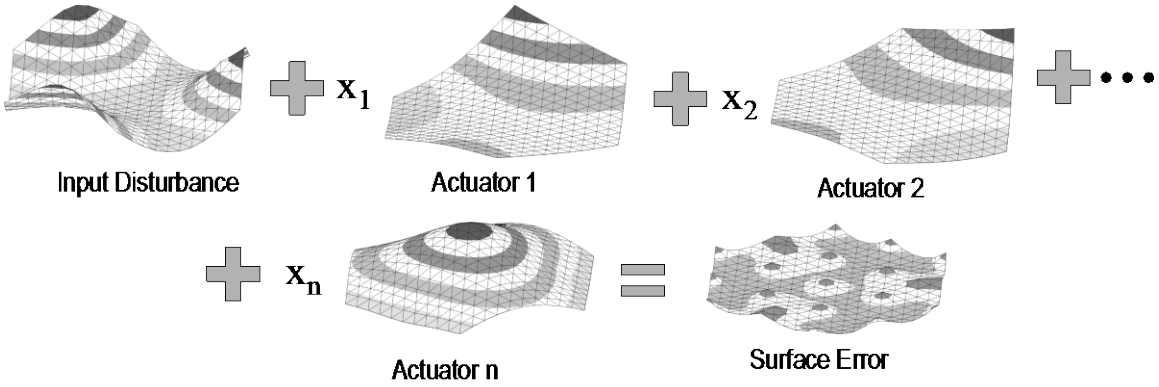

Figure 8: Pictorial equation demonstrating the process of adaptive control simulation.

Such analysis capability may be extended to consider the following design issues: actuator failure studies, control of surface slopes, and the effect of actuator resolution using Monte Carlo methods.[4]

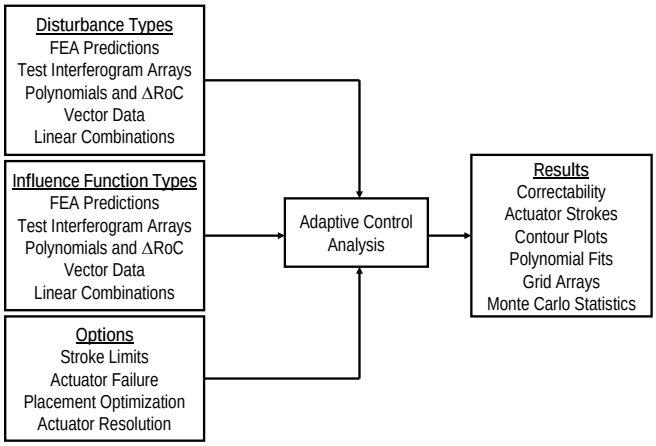

Figure 9: Flowchart of adaptive control analysis inputs and outputs.

Figure 9 shows the inputs and outputs for adaptive control simulation. Disturbances and influence functions may be defined in a variety of ways including FEA results and test data. These various form of inputs may be scaled and combined to provide complete user freedom. For example, influence functions predicted by FEA may be used to simulate correction of test data represented by interferogram arrays. If a gravity shift between the test and operation states is involved then a 1g analysis backout could be applied to the test data before correction simulation is performed. The adaptive analysis feature is also useful in the simulation of stress-optic polishing.[5]

3.2 Actuator Placement Optimization

Actuator placement optimization is a useful design feature to obtain optimum locations for actuators used in an adaptively controlled optic.[6] The process employs a genetic optimization algorithm that is well-suited for such a problem of a combinatorial nature. Figure 10 shows a flow chart of the genetic optimization process. An initial population of an even number of actuator layouts is randomly selected. Fitness evaluation of each actuator layout in the initial population is performed by computing the corrected surface RMS error of each actuator layout. The convergence step is bypassed on the first iteration. Three processes known as mating selection, crossover and mutation are then performed to find new actuator layouts with superior adaptively controlled correctability. The process loops until a convergence criterion is achieved.

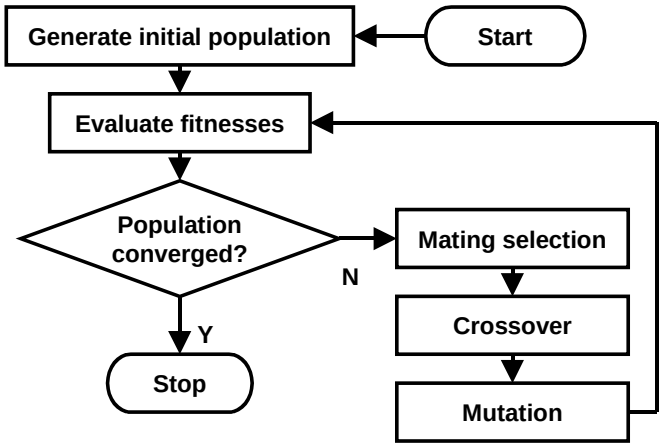

Figure 10: Flowchart of a genetic optimization algorithm that may be employed in actuator layout optimization.

Actuator placement optimization was run on a single segment of the mirror array shown in Figure 11(a). Allowable actuator locations were specified as shown in Figure 11(b). The shaded locations indicate independent locations while the unshaded locations are locations dependent on inclusion of the independent locations. This was done to enforce symmetry in the actuator layout designs considered in the optimization process.

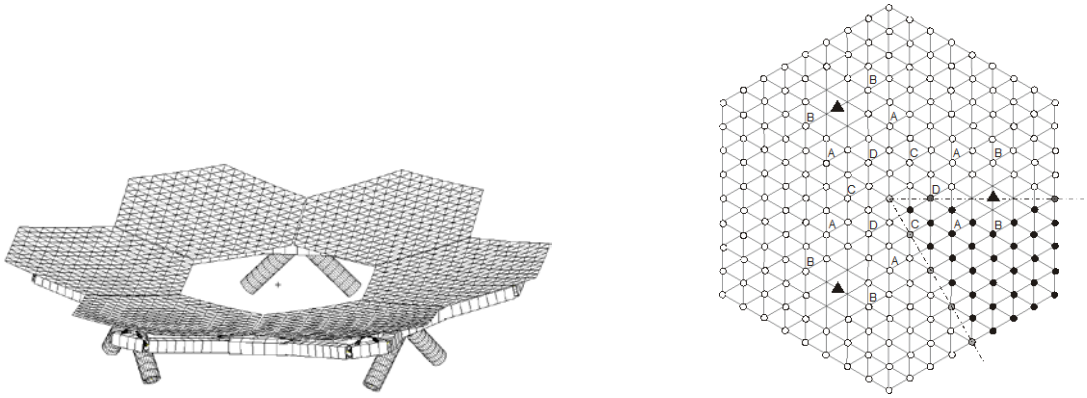

(a) (b)

Figure 11: Finite element models of (a) mirror array and (b) single segment. The plot of the single segment in (b) shows the location of candidate actuators used in actuator placement optimization. The circles indicate force actuators while the triangles indicate displacement actuators at mount points.

Two load conditions were considered: a gravity reorientation and a nonuniform temperature change. Actuator layout optimization was performed in three ways. The first was to consider correction of the disturbance of only the gravity induced disturbance. The second optimization was to consider only the temperature change induced disturbance. The third optimization was to consider both disturbances where the figure of merit in comparing actuator layouts was the larger of the corrected surface RMS errors of the two load cases. The optimum actuator layouts resulting from the analysis are shown in Figure 12.

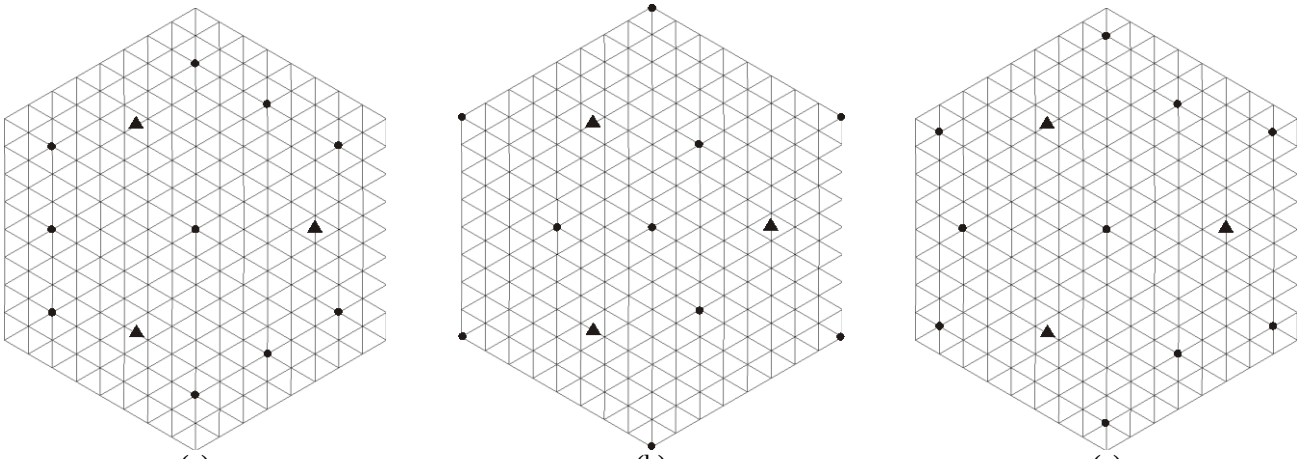

(a) (b) (c)

Figure 12: Optimum actuator layouts found for (a) gravity induced disturbance, (b) thermal induced disturbance and (c) both gravity induced and thermal induced disturbances. The circles indicate force actuators while the triangles indicate displacement actuators at mount points.

The uncorrected surface deformations for the gravity induced disturbance and the thermally induced disturbance are shown in Figure 13.

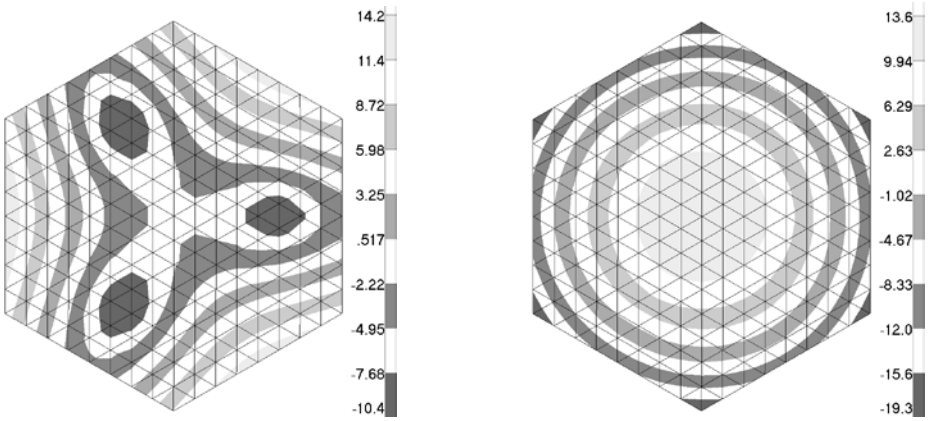

(a) (b)

Figure 13: Predictions of uncorrected surface deformation on one segment due to (a) gravity reorientation and (b) temperature change.

Predictions of the corrected surface errors for each actuator layout and disturbance are shown in Table 1. The reader should note that there is some loss in correctability for each disturbance as a result of trying to optimize a layout for both disturbances.

Table 1: Summary of Corrected Surface Error Predictions

	Corrected Surface RMS Error Predictions (He-Ne waves)		
Disturbance	Optimized for Gravity	Optimized for Thermal	Optimized for Both
Gravity	0.779	1.296	1.207
Thermal Change	1.484	0.821	1.030

Figure 14 shows contour plots of the corrected surface predictions for each of the actuator layouts optimized for each disturbance. Figure 15 shows contour plots of the corrected surface predictions for the actuator layout optimized for both disturbances.

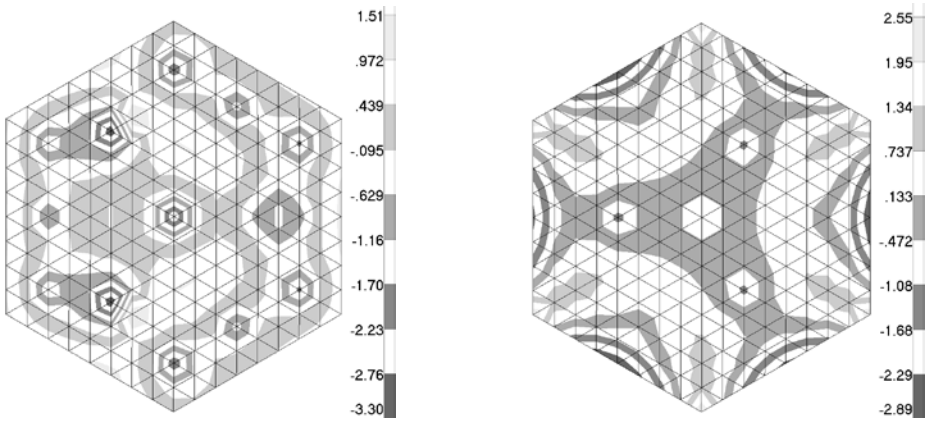

(a) (b)

Figure 14: Predictions of corrected surface deformation on one segment due to (a) gravity reorientation and (b) temperature change. Corrected surface predictions use actuator layouts optimized for each load case.

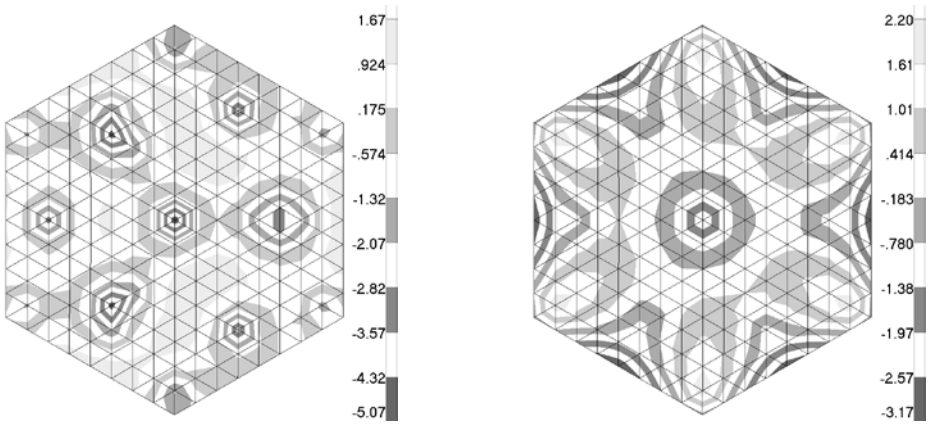

(a) (b)

Figure 15: Predictions of corrected surface deformation on one segment due to (a) gravity reorientation and (b) temperature change. Corrected surface predictions use actuator layouts optimized for both load cases.

4.0 SURFACE DEFORMATION ANALYSIS

The usual goal of surface deformation analysis is to characterize the deformations of optical surfaces so that they may be imported into an optical analysis model for performance evaluation. The two principal methods of characterizing surface deformations of optical surfaces are polynomial fitting and array interpolation. When applied to segmented array systems surface fitting may be conducted on the full array with polynomials centered on the parent vertex or individual segments may be fit with segment centered polynomials.[7] Generally, polynomial fits to the full array are poor representations of the behavior of the array because the polynomials are insufficient to accurately represent the discontinuous behavior of the segmented array. Therefore, polynomial fitting in usually performed on each segment individually as shown in Figure 16. Interpolation of surface deformations to rectangular arrays is generally used in cases where polynomial fitting is insufficient to represent the surface deformation of a segment as might be the case with significant quilting deformation of a lightweighted mirror segment. As part of the characterization process, the rigid-body motions of the segments' optical surfaces may also be subtracted prior to the fitting or interpolation process. These rigid-body motion are generally treated separate from the polynomial fit or interpolated array data and are imported to the optical analysis tool as such.

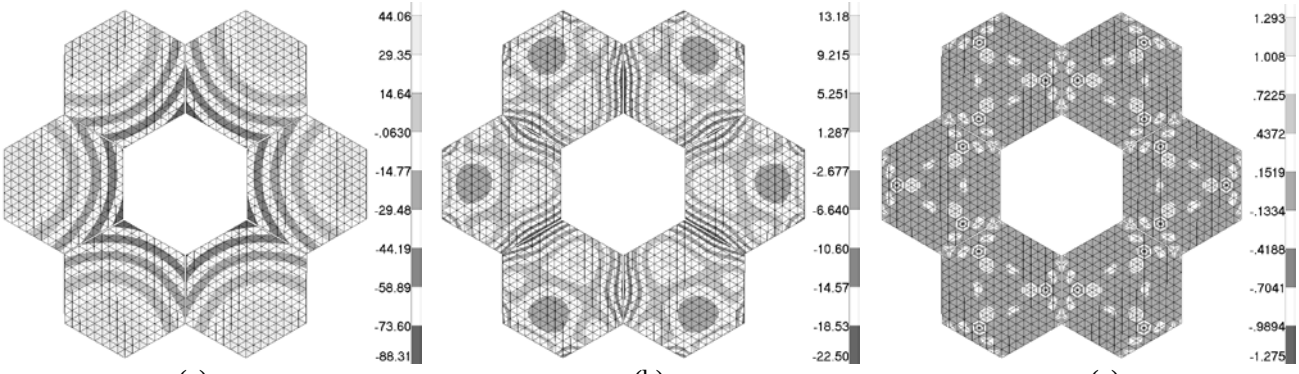

(a) (b) (c)

Figure 16: Contour plots of (a) thermally induced surface deformation, (b) residual surface deformation after polynomial fitting array with a single fit and (c) residual surface deformation after polynomial fitting each segment with individual fits.

5.0 SUBSTRATE OPTIMIZATION

Optimization of optical substrates may be performed through the use of custom response quantities through either multi-point constraint equations or an external response subroutine. Quantities linearly dependent on the finite element displacement vector such as surface rigid body motions and best-fit polynomial coefficients may be written as linear constraint equations. Quantities non-linearly related to the finite element displacement vector such as surface RMS error and peak-to-valley surface error must be written using more complex features such as NASTRAN's DRESP2 entry.[8] An external response capability allows adaptively corrected surface RMS to be computed as a response.[9] Once such responses may be computed within the finite element analysis tool then they may be used as a constraint or objective function. When using a linear optic model, the external subroutine may be extended to compute system level wavefront error. Figure 17 shows the optimization of a lightweighted adaptive mirror segment incorporating a variable shape of the ribs. The optimized design achieves a corrected surface RMS error of 0.07 He-Ne waves compared to the baseline corrected surface RMS error of 0.20 He-Ne waves.

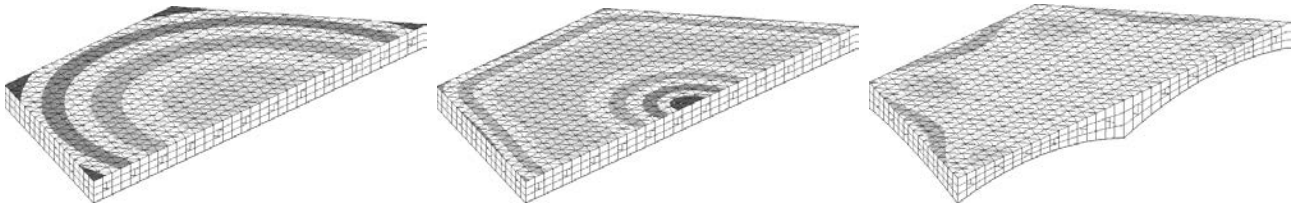

(a) (b) (c)

Figure 17: Contour plots of (a) uncorrected surface deformation of the baseline segment design (1.58 He-Ne waves surface RMS error), (b) corrected surface deformation of the baseline segment design (0.20 He-Ne waves surface RMS error) and (c) corrected surface deformation of the optimized segment design (0.07 He-Ne waves surface RMS error).

The above example could also have been performed on a constant depth design with core rib thicknesses used as design variables.

6.0 LINE-OF-SIGHT ERROR AND JITTER

Line-of-sight error is a type of optical performance degradation as shown in Figure 18. Line-of-sight error may be quantified by decentration of the image, angular deviation of the rays in image space or angular deviation of the rays in image space. Often line-of-sight error is computed with a single ray traced through the disturbed system. When using a single ray to compute line-of-sight error generally only the rigid body motions of the surfaces are used in order to eliminate the local effects of elastic surface deformation. Line-of-sight error may be computed for static disturbances or dynamic disturbances. Line-of-sight error for dynamic disturbances may be decomposed into jitter and drift components using the integration time of the sensor.[10] The jitter component may be subsequently used to compute the effect on the optical modulation transfer function (MTF).[11]

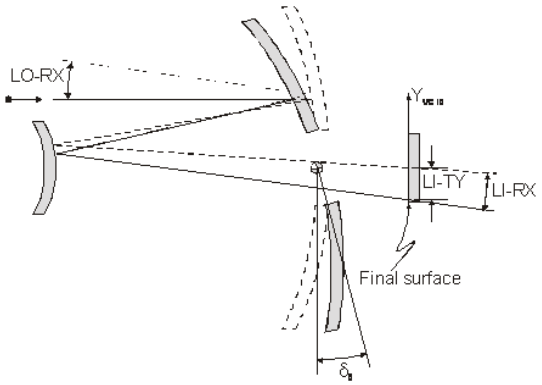

Figure 18: Illustration of line-of-sight error in an optical system.

It is important to note that computation of optical performance metrics induced by random vibration are not achievable within the features of a finite element analysis tool alone. Nodal displacement results from a random response analysis performed in FEA do not contain the phasing information that is important to distinguish between optically different behaviors such as those shown in Figure 19.

Figure 19: The surface RMS of the piston motion shown in (a) is equal to the surface RMS of the elastic motion shown in (b). When performing random response within a commercial finite element program such specific behaviors cannot be distinguished rendering useless the employment of FEA without other specialized software for opto-mechanical analysis.

Specialized techniques can be employed to conduct vibration analysis using only the natural frequency analysis results from an FEA. These techniques involve decomposing the modal analysis data into rigid body motions, surface RMS error, and line-of-sight results before forced response analysis is performed outside of the FEA software. Such methods also allow decomposition of the results by their modal contribution allowing engineers to understand which dynamic modes are contributing to optical performance degradation.

The line-of-sight error may also be expressed as multi-point constraint equations for use as a design response in design optimization within the finite element tool.

7.0 SUMMARY

The unique demands associated with analysis and design of adaptively controlled segmented optics require special attention and customized tool development in order to achieve optimum performance. Analysis issues relating to surface characterization, simulation of adaptive control, and finite element model construction present accuracy and efficiency challenges that are surpassable through appropriate methods. Other issues relating to design development such as the optimum placement of actuators and the structural design of the substrate are areas where customized techniques can enhance optical performance significantly.

REFERENCES

1. *SigFit Reference Manual*, Sigmadyne, Inc., Rochester, NY, (2011).
2. Doyle, K., Genberg, V., Michels, G., *Integrated Optomechanical Analysis 2nd Ed*, SPIE Press (pending publication Aug 2012).
3. Doyle, K., Genberg, V., Michels, G., "Integrated optomechanical analysis for adaptive systems," Proc. SPIE 5178-5, (2003).
4. Genberg, V., Michels, G., Bisson, G., "Optomechanical tolerancing with Monte Carlo techniques," Proc. SPIE 8125-10, (2011).
5. Genberg, V., Michels, G., Bisson, G., "Optomechanical analysis in the fabrication of conformal and free-form optics," Proc. SPIE TD-07-33, (2011).
6. Michels, G., Genberg, V., Doyle, K., and Bisson, G., "Design optimization of actuator layouts of adaptive optics using a genetic algorithm," Proc. SPIE 5877-22, (2005).
7. Genberg, V., Michels, G., "Optomechanical analysis of segmented/adaptive optics," Proc. SPIE 4444-10, (2011).
8. Genberg, V., "Optical Performance Criteria in Optimum Structural Design," Proc. SPIE 3786-29, (1999).
9. Michels, G., Genberg, V., Doyle, K., Bisson, G., "Design optimization of system level adaptive optical performance", Proc. SPIE 5867-25, (2005).
10. Lucke, R. L., Sirlin, S. W., San Martin, A. M., "New Definitions of Pointing Stability: AC and DC Effects," The Journal of Astronautical Sciences, Vol. 40, No.4, Oct-Dec 1992, pp 557-576.
11. Genberg, V., Michels, G., Doyle, K., "Integrated modeling of jitter MTF due to random loads," Proc. SPIE 8127-16, (2011).